Characterization of the Complex of a Trifluoromethyl-Substituted Shikimate-Based Bisubstrate Inhibitor and 5-Enolpyruvylshikimate-3-phosphate Synthase by REDOR NMR†

Lynda M. McDowell,‡ Daniel R. Studelska,‡,|| Barbara Poliks,§ R. D. O'Connor,‡ and Jacob Schaefer*,‡

Department of Chemistry, Washington University, St. Louis, Missouri 63130, Department of Physics, Binghamton University, Binghamton, New York 13902

Received February 11, 2004; Revised Manuscript Received March 31, 2004

ABSTRACT: A combination of $^{15}N\{^{19}F\}$, $^{31}P\{^{15}N\}$, and $^{31}P\{^{19}F\}$ rotational-echo double-resonance NMR has been used to characterize the conformation of a bound trifluoromethylketal, shikimate-based bisubstrate inhibitor of 5-enolpyruvylshikimate-3-phosphate synthase. The solid-state NMR experiments were performed on the complex formed in solution and then lyophilized at low temperatures in the presence of stabilizing lyoprotectants. The results of these experiments indicate that none of the side chains of the six arginines that surround the active site forms a compact salt bridge with the phosphate groups of the bound inhibitor.

The 46-kDa enzyme 5-enolpyruvylshikimate-3-phosphate (EPSP)[1] synthase catalyzes the reversible condensation of shikimate-3-phosphate (S3P) and phosphoenolpyruvate (PEP) to form EPSP in the synthesis of aromatic amino acids in plants and microorganisms (*1*). This reaction is inhibited by the commercial herbicide *N*-(phosphonomethyl)glycine (glyphosate or Glp), $HO_3PCH_2NHCH_2COOH$, which, in the presence of S3P, binds to EPSP synthase and forms a stable, ternary complex (*2*). A crystal structure of the ternary complex has been published recently (*3*) that shows Glp in an extended conformation proximate to S3P. Both Glp and S3P are negatively charged and are stabilized in the binding site by the side chains of a histidine, three lysines, and five arginines.

Rotational-echo double-resonance (REDOR) NMR experiments have also been performed on the ternary complex of EPSP synthase (*4*−*6*). The results of these experiments are in agreement with the X-ray crystal structure, except for the positions of the side chains of some of the arginines near the binding site (*6*). In particular, REDOR unambiguously shows a closer approach of the guanidino nitrogens and the phosphate of S3P, the carboxyl of Glp, and especially the phosphonate of Glp (*6*) than is seen by the X-ray analysis. On the basis of the observed narrow ^{31}P resonance line widths (*5*), both S3P and Glp are ordered in the binding site.

An extended rather than bent conformation of Glp in the EPSP synthase binding site means that the S3P−Glp combination in the ternary complex is not a close mimic of the S3P−PEP tetrahedral intermediate (*7*). However, various covalently linked, shikimate-based bisubstrate inhibitors (SBBIs) are close mimics (*8*). The nanomolar binding affinities of these ligands suggest the possibility of salt-bridge matches with the surrounding lysine and arginine side chains. No crystal structures have been reported for these complexes. This paper reports the results of REDOR experiments performed on a trifluoromethyl-substituted SBBI (CF_3−SBBI) complexed to [$^{15}N_2$]Arg−EPSP synthase. The REDOR results show that the arginines do not form salt bridges to the phosphate groups of CF_3−SBBI. This result is not consistent with the notion that a function of the enzyme is to stabilize the transition state.

EXPERIMENTAL PROCEDURES

Labeled EPSP Synthase. Wild-type *Escherichia coli* EPSP synthase was overexpressed in an *E. coli* strain auxotrophic for arginine (ATTC 23790) to increase the incorporation of L-arginine-guanidino-$^{15}N_2$ (Cambridge Isotope Laboratories, Andover, MA) into the enzyme. The expression system (*6*) was made by transformation of ATTC 23790 with pMON5537. The transformed cells were stored as frozen glycerol stocks. A colony of these cells was selected from a 37 °C, 18-h agar plate made with Luria-Bertani media containing ampicillin at 200 μg/mL (LB/AMP). The colony was transferred to 6 mL of liquid LB/AMP and incubated overnight in an orbital shaking incubator at 225 rpm and 37 °C. These cells were used to inoculate two 250-mL flasks each containing 50 mL of unlabeled defined growth medium. At mid-log phase (OD_{600} = 1.2), 10-mL aliquots of this

† This work was supported by NIH Grant EB01964.

* To whom correspondence should be addressed. Phone: 314-935-6844. Fax: 413-935-4481. E-mail: schaefer@wuchem.wustl.edu.

‡ Washington University.

§ Binghamton University.

|| Current address: Department of Pathology and Immunology, Washington University School of Medicine, St. Louis, MO 63110.

[1] Abbreviations: ΔS, $S_0 - S$, where S and S_0 are rotational-echo double-resonance signal intensities with and without dephasing pulses, respectively; EPSP, 5-enolpyruvylshikimate-3-phosphate; Glp, *N*-(phosphonomethyl)glycine; HEPES, *N*-[2-hydroxyethyl]piperazine-*N*′-[2-ethanesulfonic] acid; PEG, poly(ethylene glycol); PEP, phosphoenolpyruvate; REDOR, rotational-echo double resonance; SBBI, shikimate-based bisubstrate inhibitor; S3P, shikimate-3-phosphate; CF_3−SBBI, trifluoromethylketal−SBBI.

10.1021/bi049685w CCC: $27.50
Published on Web 05/07/2004

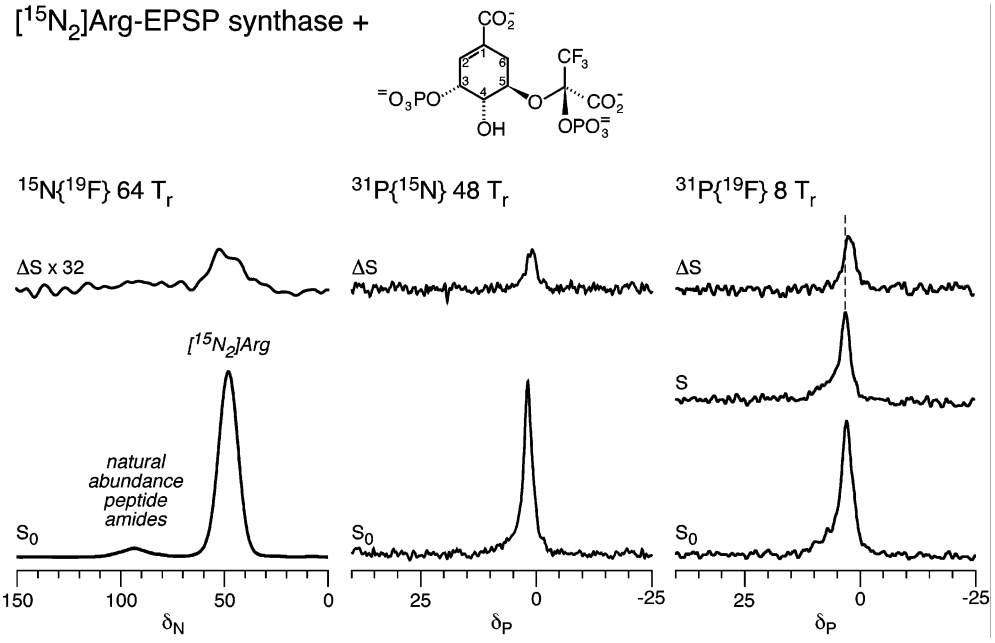

FIGURE 1: $^{15}N\{^{19}F\}$ (left), $^{31}P(^{15}N\}$ (middle), and $^{31}P\{^{19}F\}$ (right) REDOR dephasing ($\Delta S/S_0$) for the complex of CF_3−SBBI (inset) with [$^{15}N_2$]Arg−EPSP synthase. The REDOR differences are shown at the top of the figure and the full echoes, at the bottom. The $^{31}P\{^{19}F\}$ dephased-echo spectrum (S) is also shown (right). The spectra on the left resulted from the accumulation of 375 072 scans, those in the middle, 54 900 scans, and those on the right, 22 096 scans. Magic-angle spinning was at 5 kHz.

growth were used to inoculate 10 1000-mL flasks each containing 400 mL of the same defined medium. The bacteria from the 1000-mL flasks were pelleted at mid-log phase. Each pellet was resuspended in 400 mL of a defined medium containing L-arginine-guanidino-$^{15}N_2$. The resuspended cells, returned to the 1000-mL flasks, were incubated, as before, 30 min (to $OD_{600} = 1.6$) before EPSP synthase overexpression was induced by addition of nalidixic acid at 75 μg/mL. Incubation continued for 9.5 h before the cells were pelleted and frozen. Protein purification was as described previously (*5*). The yield of the purified enzyme was 105 mg/L of the labeled medium.

The unlabeled defined medium contained 12.8 mg/mL $Na_2HPO_4 \cdot 7H_2O$, 3 mg/mL KH_2PO_4, 0.5 mg/mL NaCl, 77.8 μg/mL thiamine−HCl, 6 μg/mL $FeCl_3$, 100 μg/mL ampicillin, 4 mg/mL D-glucose, 1 mg/mL NH_4Cl, 0.44 μg/mL $ZnSO_4 \cdot 7H_2O$, 0.78 μg/mL $Na_2MoO_4 \cdot 2H_2O$, 0.892 μg/mL $CuSO_4 \cdot 5H_2O$, 0.22 μg/mL H_3BO_3, 0.56 μg/mL $MnSO_4 \cdot H_2O$, 0.78 μg/mL $CoCl_2 \cdot 6H_2O$, 2 mM $MgSO_4$, 100 μM $CaCl_2$, 225 μg/mL L-alanine, 37.5 μg/mL L-arginine, 100 μg/mL L-asparagine, 125 μg/mL L-aspartate, 37.5 μg/mL L-cysteine, 100 μg/mL L-glutamic acid, 100 μg/mL L-glutamine, 250 μg/mL glycine, 37.5 μg/mL L-histidine, 125 μg/mL L-isoleucine, 250 μg/mL L-leucine, 100 μg/mL L-lysine, 75 μg/mL L-methionine, 75 μg/mL L-phenylalanine, 100 μg/mL L-proline, 125 μg/mL L-serine, 160 μg/mL L-threonine, 16 μg/mL L-tryptophan, 75 μg/mL L-tyrosine, and 160 μg/mL L-valine. The medium was adjusted to pH 7 after the dropwise addition of $MgSO_4$ and $CaCl_2$. These salts were added last, at 98% of the final volume. The labeled defined medium was similar except that it contained 115 μg/mL L-[guanidino-$^{15}N_2$]arginine instead of unlabeled L-arginine, 50 μg/mL L-cysteine, and 50 μg/mL L-histidine. Isotopic enrichment was 85% as determined by solid-state NMR spin counts (*5*, *10*).

Lyophilization of the Complex. A 140-mg aliquot of the labeled enzyme was complexed 1:1 with the CF_3−SBBI (structure *R*-5 in ref *8*; see inset of Figure 1) inhibitor of EPSP synthase ($K_{i,app} = 32$ nM, ref *7*) in a lyophilization flask. The final step in catalysis by EPSP synthase is the release of products (EPSP and HPO_4^{-2}). The presence of the CF_3 group of the SBBI and the resulting unavailability of a transferable proton block the final step. The enzyme and inhibitor were incubated for 30 min at 4 °C, each at 101 μM, at a final volume of 30 mL. The lyophilization buffer was 2 mM MOPS, 1 mM DTE, 1% (w/v) PEG 8000, and 20 mM trehalose at pH 7.24. After the incubation at 4 °C, the flask was gradually cooled until the sample reached −7 °C. After ice-crystal formation was apparent, the sample was further cooled to −30 and −70 °C before it was lyophilized. The NMR sample was lyophilized at reduced temperatures ranging from −80 to −30 °C to prevent sample melt-back before completion of the lyophilization at room temperature (*9*).

Dipolar Recoupling. REDOR was used to restore the dipolar coupling between heteronuclear pairs of spins that is removed by magic-angle spinning (*11*). REDOR experiments are always done in two parts, once with rotor-synchronized dephasing pulses (S) and once without (S_0). The dephasing pulses change the sign of the heteronuclear dipolar coupling, and this interferes with the spatial averaging resulting from the motion of the rotor. The difference in signal intensity ($\Delta S = S_0 - S$) for the observed spin in the two parts of the REDOR experiment is directly related to the corresponding distance to the dephasing spin (*12*). REDOR has found an application in the characterization of binding sites of proteins (*4*, *5*, *13*) and in the analysis of heterogeneous biological materials such as amyloid plaques (*14*), membrane protein helical bundles (*15*, *16*), insect cuticle (*17*), bacterial cell walls (*18*), and spider silk (*19*).

Data Acquisition. REDOR NMR was performed using 4-frequency transmission-line probes (*20*) having a 14-mm long, 9-mm inside-diameter analytical coil and a Chemagnetics/Varian stator and spinner housing. Lyophilized samples

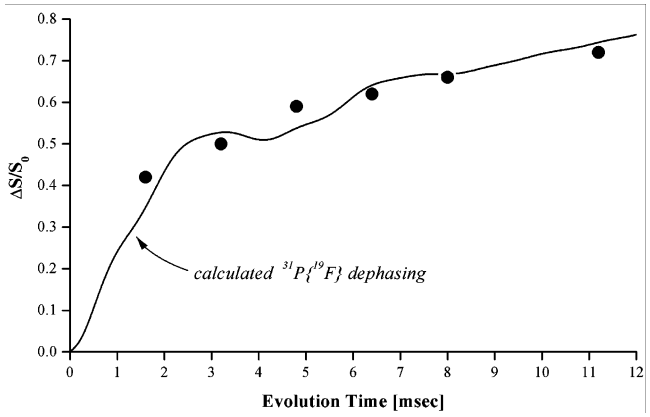

FIGURE 2: $^{31}P\{^{19}F\}$ REDOR dephasing ($\Delta S/S_0$) for the complex of CF_3−SBBI of Figure 1 with [$^{15}N_2$]Arg−EPSP synthase. Experimental dephasing (for the sum of the ring and nonring phosphate ^{31}P signal intensity) is represented by (●). Initial-distance estimates for modeling came from an RMSD best fit assuming a nonring phosphate ^{31}P to CF_3 distance of 3.8 Å and varying (i) the ring-phosphate ^{31}P to CF_3 distance and (ii) the percentage contribution to the total signal intensity by the ring-phosphate ^{31}P (initially 50%). The calculation (—) is for the geometry of the model in Figure 4. The nonring phosphate to CF_3 distance is 8.3 Å. After 56 rotor cycles, the best-fit ring-phosphate percentage increased to 70%. This change in relative contributions to $\Delta S/S_0$ for the ring and nonring phosphates indicates a difference in the ^{31}P echo lifetimes. Magic-angle spinning was at 5 kHz.

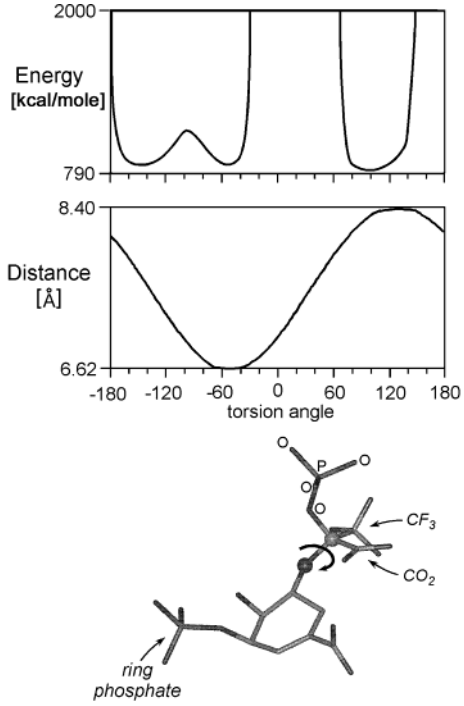

FIGURE 3: (Top) Sum of van der Waals and Coulombic energies of CF_3−SBBI as a function of the rotation about the oxygen-tetrahedral carbon bond of the inhibitor (see bottom inset). (Middle) ^{31}P-^{19}F distance from the center of the CF_3 triangle to the phosphorus of the shikimate ring as a function of the same rotation angle. (Bottom) CF_3−SBBI.

were contained in Chemagnetics/Varian 7.5-mm outside-diameter zirconia rotors. The rotors were spun at 5000 Hz with the speed under active control to within ±2 Hz. Experiments with ^{19}F dephasing were done using a 4.7-T magnet (200 MHz for protons); all other experiments were done using a 7.05-T magnet (300 MHz for protons). The 200-MHz spectrometer was controlled by a Tecmag pulse programmer and the 300-MHz spectrometer, by a Chemagnetics console. Radio frequency pulses were produced by Kalmus, ENI, and American Microwave Technology power amplifiers. The π-pulse lengths were 10 μs for ^{15}N, ^{31}P, and ^{19}F. The accuracy of distance measurements using ^{19}F-dephasing pulses was confirmed using a ^{13}C-, ^{15}N-, and ^{19}F-labeled peptide (*21*). Standard XY-8 phase cycling (*22*) was used for all pulses. Proton−carbon cross-polarization transfers were made in 2 ms at 50 kHz. Proton dipolar decoupling was 100 kHz during data acquisition. The ^{31}P chemical-shift scale was referenced relative to external phosphocreatine and the ^{15}N chemical-shift scale, to external ammonium sulfate.

Molecular Modeling. The closed REDOR structure and REDOR-refined X-ray structure (*6*) of liganded EPSP synthase (with Phe172 replaced by Trp172, F172W) were used to build the models of the EPSP synthase−CF_3−SBBI binary complex using Insight II software (Accelrys, Inc., San Diego, CA). A sequence of dynamics steps was applied (using consistent valence force fields and algorithms from Accelrys, Inc.) with the distances between ^{31}P and ^{19}F of the ligand and selected arginine residues of the enzyme restrained to the ranges measured by REDOR. The structure was minimized so that the derivative of the total energy was less than 1 kcal mol^{-1} Å^{-1}.

RESULTS AND DISCUSSION

Proximity of Arginines and CF_3. The ^{15}N full-echo spectrum of CF_3−SBBI−[$^{15}N_2$]Arg−EPSP synthase (bottom left of Figure 1) has just two peaks: a major ^{15}N-labeled guanidino-nitrogen peak near 50 ppm (arising from 21 arginine residues) and a minor natural-abundance ^{15}N peptide peak at 95 ppm. The ^{15}N spin count (*5*, *10*) of the full-echo spectrum corresponds to approximately 85% ^{15}N isotopic enrichment for the guanidino nitrogens. The $^{15}N\{^{19}F\}$ $\Delta S/S_0$ of this complex (left of Figure 1) is about 1% after 12.8 ms of dipolar evolution (64 rotor cycles with magic-angle spinning at 5 kHz). If just one arginine was less than 5 Å from the −CF_3, the observed dephasing would be about 5% (total dephasing for 1 of 21 arginines). A 1% value means that the guanidino nitrogens of the nearest binding-site arginine side chain must be more than 7 Å from the CF_3 moiety of the bound SBBI. This is a lower limit based on the assumption that the nearest neighbor is responsible for all of the dephasing. If more arginine nitrogens contribute to the dephasing (which seems likely considering the complicated line shape for ΔS), then the distance to the nearest nitrogen will increase. (This point will be discussed in more detail in the modeling section, below.)

Two ^{31}P Chemical Shifts. The 8-T_r $^{31}P\{^{19}F\}$ REDOR difference (ΔS) of CF_3−SBBI−[$^{15}N_2$]Arg−EPSP synthase represents about half of the total intensity of the full-echo signal (S_0), and the dephased echo (S) represents the other half (right of Figure 1). There is about a 1-ppm shift difference between ΔS and S (dotted line of Figure 1). The nonring phosphate is just three bonds away from the CF_3 group (compared to seven bonds for the ring phosphate), and its signal is therefore necessarily the first to dephase under a dipolar evolution as short as 8 rotor cycles. Thus, the nonring phosphate is assigned to the higher-field component of S_0 and the ring phosphate, to the lower-field component. The nonring ^{31}P line width is more than 200 Hz

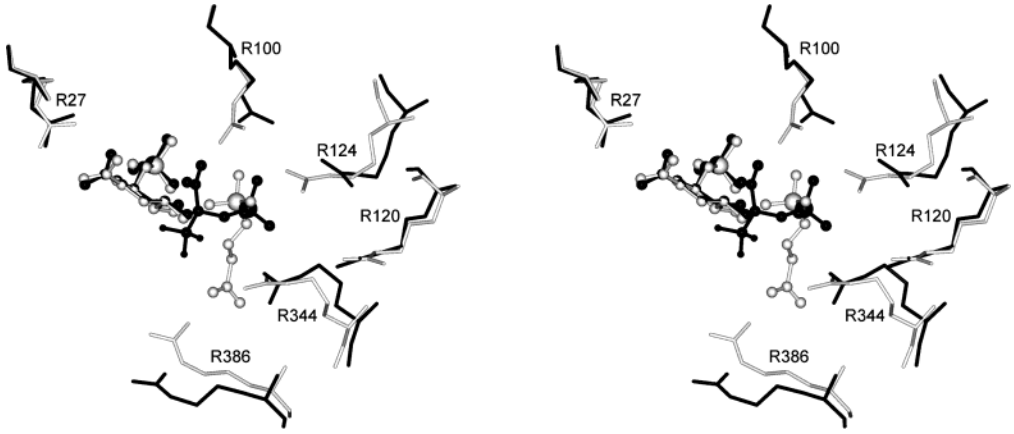

FIGURE 4: Stereoviews of the models of two different complexes. The REDOR model of the binding site of EPSP synthase complexed to S3P and Glp is shown in gray and that to CF_3−SBBI of Figure 1, in black. The P atoms are the large spheres; no hydrogens are displayed. Only the positions of the six arginines of EPSP synthase lining the binding site are shown. The shikimate rings are overlayed. The coordinates of the model in gray were obtained from the REDOR model of ref *6*. The coordinates of the model in black were obtained from a molecular dynamics simulation and energy minimization (with the model in gray providing the starting coordinates), restrained by the ^{19}F-^{15}N and ^{31}P-^{15}N distances determined by the REDOR results of Figure 1 (left) and Table 1, respectively.

Table 1: $^{31}P\{^{15}N\}$ REDOR Dephasing ($\Delta S/S_0$) for Complexes of $[^{15}N_2]$Arg−EPSP Synthase[a] with Either S3P and Glp or CF_3−SBBI

	number of rotor cycles[b]		
^{31}P observed	32	48	64
Glp (54% ^{15}N)[c] phosphonate	0.48	0.71	0.75
Glp(85% ^{15}N)[d] phosphonate	0.73	0.94	0.97
CF_3−SBBI (obs)[e] nonring phosphate	0.30	0.43	0.60
CF_3−SBBI (calc)[e,f] nonring phosphate	0.13	0.27	0.43
S3P (54% ^{15}N)[c] phosphate	0.03	0.08	0.14
S3P (85% ^{15}N)[d] phosphate	0.06	0.14	0.23
CF_3−SBBI (obs)[e] ring phosphate	0.10	0.15	0.20
CF_3−SBBI (calc)[e,f] ring phosphate	0.05	0.11	0.18

[a] ^{15}N isotopic enrichment of the guanidino nitrogens was 54% for the EPSP synthase used for the complex with S3P and Glp and 85% for the complex with CF_3−SBBI. [b] Magic-angle spinning was at 5000 Hz. [c] Observed dephasing from refs *5* and *6*. [d] Dephasing expected for 85% ^{15}N isotopic enrichment of arginine guanidino nitrogens. [e] This paper. [f] On the basis of the REDOR model of Figure 4 and Table 1.

Table 2: ^{31}P-$[^{15}N_2]$Arg−EPSP Synthase Distances (in Å) for the CF_3−SBBI Models of Figure 5

		REDOR model (black)[a]		REDOR-refined X-ray (gray)[b]	
nitrogen		nonring P	ring P	nonring P	ring P
R27	NH1	11.4	8.5	11.2	8.6
	NH2	10.7	8.0	10.7	9.2
R100	NH1	6.8	5.4	7.8	5.2
	NH2	6.0	7.4	9.2	7.4
R120	NH1	6.7	15.1	12.3	13.8
	NH2	8.5	16.9	10.6	12.1
R124	NH1	4.8	10.6	4.9	9.1
	NH2	5.7	12.4	5.5	7.4
R344	NH1	8.1	9.7	6.9	9.6
	NH2	8.5	8.5	7.4	11.4
R386	NH1	11.0	11.4	9.4	13.5
	NH2	11.6	12.1	10.1	13.0

[a] PDB code for initial coordinates 1Q0I. [b] PDB code for initial coordinates 1Q0J.

at 81 MHz, which suggests some conformational heterogeneity in the CF_3−SBBI binding site (*5*). A weak, broad, low-field shoulder on S and S_0 is due to ^{31}P that is not assigned.

The $^{31}P\{^{19}F\}$ $\Delta S/S_0$ jumps to about 0.5 after only 8 rotor cycles and then increases slowly with an increasing evolution time after 8 T_r (Figure 2). The initial dephasing is due to the proximity of the nonring phosphate to the CF_3 group. The slower increase in dephasing after 8 T_r arises from the weak coupling of the distant ring-phosphate ^{31}P and corresponds to a distance of approximately 8.3 Å to the CF_3. This distance is consistent with the calculated estimates of the van der Waals and Coulombic energy for the SBBI as a function of the rotation about the oxygen-tetrahedral carbon bond of the SBBI (Figure 3, torsion angle of ±120°).

Proximity of Arginines and ^{31}P. Ring and nonring phosphate signals have a combined $^{31}P\{^{15}N\}$ $\Delta S/S_0$ of about 20% after 48 rotor cycles (center of Figure 1). Because the center of the ΔS spectrum is shifted slightly upfield, there is more dephasing for the nonring ^{31}P than for the ring ^{31}P. Using spectral deconvolution based on the shifts and line widths determined by the $^{31}P\{^{19}F\}$ dephasing, we estimate $\Delta S/S_0 = 0.15$ for the nonring phosphate and 0.25 for the ring phosphate after 48 T_r with 5-kHz spinning (Table 1). The deconvolution is difficult, and the errors are substantial (±0.05). After 64 T_r, the dephasing for the S3P part of the CF_3−SBBI complex and S3P in the S3P−Glp−EPSP synthase ternary complex are about the same (Table 1), indicating similar positioning relative to nearby arginines. However, this is not the situation for the nonring phosphate ^{31}P of the CF_3−SBBI complex. The observed dephasing after 32 and 48 T_r for the nonring ^{31}P is less than half of the dephasing for the Glp ^{31}P in the S3P−Glp−$[^{15}N_2]$Arg−EPSP synthase ternary complex, after adjustment for ^{15}N isotopic enrichment (Table 1). Thus, the nonring phosphate in the CF_3−SBBI complex cannot be close to any of the five or six arginine side chains that line the binding site.

Model of the Binding Site. The strong ^{31}P-^{15}N dipolar coupling for the phosphonate of S3P−Glp−$[^{15}N_2]$Arg−EPSP synthase is the result of an effective salt bridge with R100 (*6*). R124 is also close by. The relatively weak ^{31}P-^{15}N dipolar coupling for the nonring phosphate of CF_3−SBBI−$[^{15}N_2]$-Arg−EPSP synthase means that the PEP-like component of the SBBI has shifted away from R100 and R124. A molecular dynamics simulation (with energy minimization; see ref *6* for details) indicates that the nonring phosphate has shifted toward R386 (Figure 4). This simulation was based on the assumption that the binding site for the EPSP synthase complex with S3P−Glp (*6*) is a reasonable starting

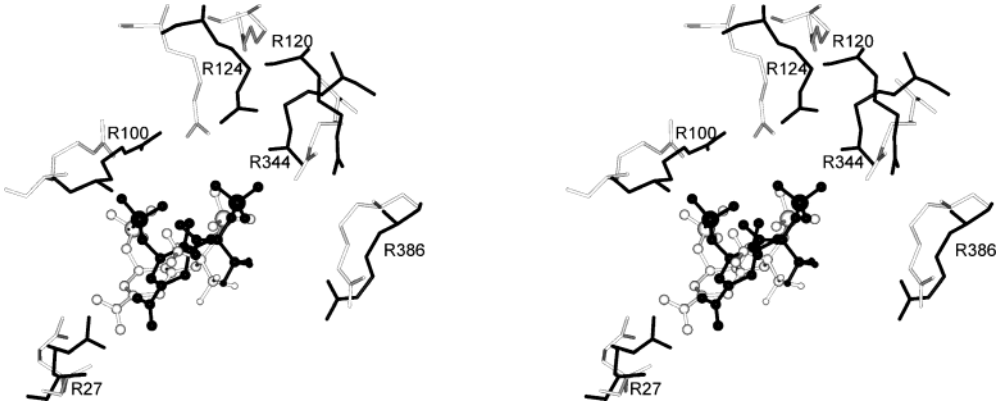

FIGURE 5: Stereoviews of two different models of the CF_3−SBBI complex. The model of the binding site of EPSP synthase complexed to CF_3−SBBI in black is the same as that shown in Figure 4 (also in black). The model in gray was obtained from a molecular dynamics simulation and energy minimization using the REDOR-refined X-ray structure of ref *6* for the starting coordinates and restrained by the ^{19}F-^{15}N and ^{31}P-^{15}N distances determined by the REDOR results of Figure 1 (left) and Table 1, respectively. The CF_3 groups in this view of the models are at the lower right, in the vicinity of Arg386. The distributions of the ^{31}P-^{15}N distances for both models (Table 2) are consistent with the experimental REDOR dephasing of Figure 1 (middle).

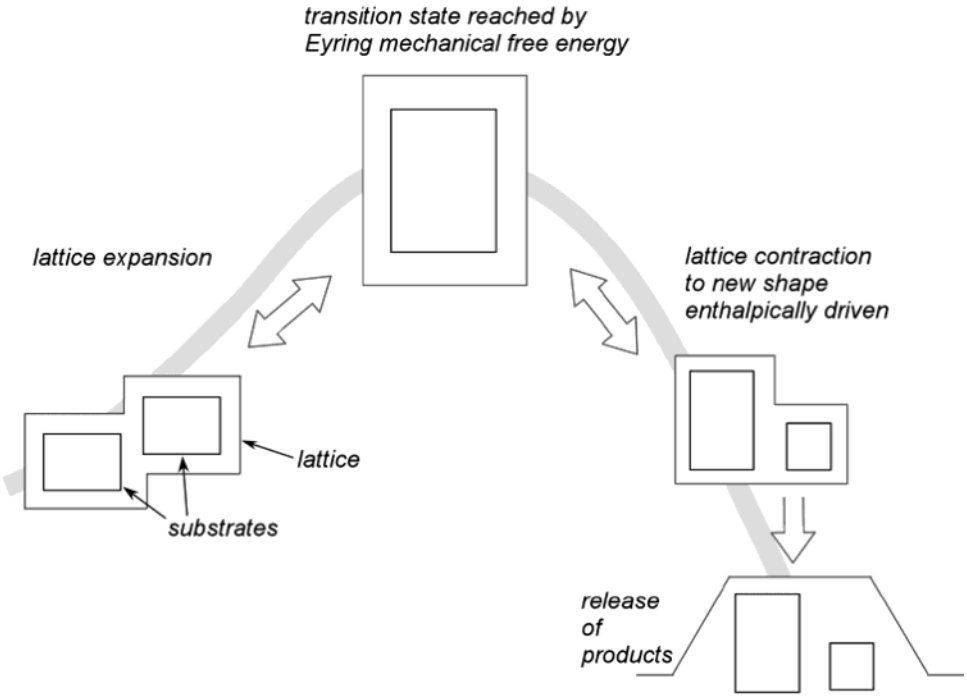

FIGURE 6: Schematic representation of bisubstrate enzyme catalysis. The pretransition state is on the left, the transition state is in the center, and the final products are on the right. The gray line indicates the total energy of the system.

point to model the complex with CF_3−SBBI. The simulation was restrained by (i) the condition that no distance between the CF_3 (center of the fluorine triangle) and a ^{15}N label can be less than 9 Å; (ii) the condition that no distance between the nonring ^{31}P and a ^{15}N label can be less than 5 Å; and (iii) the intraligand ring and nonring ^{31}P−CF_3 distances are 8.1 and 3.8 Å, respectively. The first two distance restraints are based on the REDOR results of Figure 1 and Table 1, and the intraligand distance restraints are based on the results of Figure 2.

The ^{19}F-^{15}N restraint is met by the arrangement of arginines shown in the REDOR model (black) in Figure 4. The shortest distance from ^{15}N to a CF_3 is 8.8 Å. The total calculated $^{15}N\{^{19}F\}$ dephasing for all 6 arginines (of 21) is 1%, which matches the observed value. When a ^{19}F-^{15}N distance lower limit of 8 Å was used, the total calculated $^{15}N\{^{19}F\}$ dephasing was 3%. All of the arginine ^{31}P-^{15}N distances are given in Table 2 (the shortest is 4.8 Å), and the calculated $^{31}P\{^{15}N\}$ dephasing (which is in acceptable agreement with the experimental) is given in Table 1. The intraligand distance restraints are also reasonably well-satisfied by the REDOR model of Figure 4, which has a rotational torsional angle (see Figure 3) of 104°.

On the basis of the distances of Table 2, neither R386 nor any of the other binding-site arginines has closed around the nonring phosphate of CF_3−SBBI. This sort of positioning is consistent with the observed weak ^{19}F-^{15}N dipolar coupling of the CF_3 group (left of Figure 1). Even if the histidine and the three lysines of the binding site maintain close contact, the CF_3−SBBI finds itself in a spacious catalytic center. The binding by EPSP synthase of the SBBI is therefore qualitatively different from that for S3P−Glp, in which all charged groups of the ligands are matched by charged side chains of the protein (*5*, *6*).

The binding-site arragement shown in Figure 4 is just one of many similar geometries that are allowed by the REDOR distance restraints. Another is shown in Figure 5 (in gray), with ^{31}P-^{15}N distances given in Table 2. Regardless of the details, the loose fit of all of these structures in the binding site agrees with the observed lack of dependence of the binding affinity of CF_3−SBBI on the stereochemistry of the ligand (*8*). We attribute the nanomolar-binding affinity of the negatively charged CF_3−SBBI to a combination of favorable polar enthalpic interactions with multiple positively charged lysyl and arginyl side chains, together with a reduced entropic penalty on binding (*23*).

Expanded Conformational States. We believe that the loose fit of the enzyme−substrate complex in Figure 4 is consistent with the description of enzyme catalysis via stabilization of a bisubstrate *pre*-transition state (*24*). The first step in enzyme catalysis is generally taken as the formation of an ordered intermediate in the binding site in which the two substrates have been brought together, electron density has been rearranged, but no new bonds have yet been formed (*25*). A matrix fluctuation leads to a compression of the binding site (*26*) and the beginnings of a new bond formation (*27*). This compressed, pretransition state is stabilized by strong through-space enthalpic attractions between the substrates and the protein side chains. It is the most tightly bound state in the reaction sequence but not the state with the lowest energy or highest binding affinity (*25*). (The phrase "tightly bound" in this context means accurately positioned in a single conformation with little or no local motion.) The enthalpic attractions are reduced during an expansion to the true transition state (Figure 6). This expansion is facilitated by mechanical free energy (*26*). From this view, the function of the enzyme is to provide the free energy to get the complex over the transition-state barrier, not to stabilize the transition state. The expansion of the binding site can involve entropic contributions to the free energy from distant parts of the protein matrix because of the cooperativity of packing within a folded protein. Increases in backbone mobility distant from the binding site have been discussed recently in terms of the observed distributions of X-ray Debye−Waller factors (*28*) and the observed increases of main-chain ^{15}N Overhauser enhancements (*29*).

Despite the high affinity of the binding site for the SBBI, the bisubstrate inhibitor is not tightly bound and its complex with EPSP synthase is therefore dissimilar from the pretransition state. We reach this conclusion based on the broad ^{31}P line widths (site heterogeneity) and weak through-space ^{19}F-^{15}N and ^{31}P-^{15}N dipolar couplings detected by REDOR for the arginines surrounding the SBBI (no salt bridges). The exact relation between this SBBI−enzyme complex and the true bisubstrate−enzyme transition state is not entirely clear, although we believe that both the complex and transition state have expanded conformations similar to those of Figures 4 and 5.

ACKNOWLEDGMENT

The authors thank Professor Paul A. Bartlett, Department of Chemistry, University of California at Berkeley, for the generous gift of the CF_3−SBBI and for several helpful discussions of the activity of this class of inhibitors of EPSP synthase.

REFERENCES

1. Steinrucken, H. C., and Amrhein, N. (1984) *Eur. J. Biochem. 143*, 341−349.
2. Anderson, K. S., and Johnson, K. A. (1990) *Chem. Rev. 90*, 1131−1149.
3. Schönbrunn, E., Eschenburg, S., Shuttleworth, W. A., Schloss, J. V., Amrhein, N., Evans, J. N. S., and Kabsch, W. (2001) *Proc. Nat. Acad. Sci. U.S.A. 98*, 1376−1380.
4. Studelska, D. R., Klug, C. A., Beusen, D. D., McDowell, L. M., and Schaefer, J. (1996) *J. Am. Chem. Soc. 118*, 5476−5477.
5. McDowell, L. M., Schmidt, A., Cohen, E. R., Studelska, D. A., and Schaefer, J. (1996) *J. Mol. Biol. 256*, 160−171.
6. McDowell, L. M., Poliks, B., Studelska, D. R., O'Connor, R. D., Beusen, D. D., and Schaefer, J. (2004) *J. Biomol. NMR 28*, 11−29.
7. Franz, J. E., Mao, M. K., and Sikorski, J. A. (1997) *Glyphosate: A Unique Global Herbicide*, p 521, ACS Monograph 189, Washington, D. C.
8. Alberg, D. G., Lauhon, C. T., Nyfeler, R., Fässler, A., and Bartlett, P. A. (1992) *J. Am. Chem. Soc. 114*, 3535−3546.
9. McDowell, L. M., McCarrick, M. A., Studelska, D. R., Guilford, W. J., Arnaiz, D., Dallas, J. L., Light, D. R., Whitlow, M., and Schaefer, J. (1999) *J. Med. Chem. 42*, 3910−3918.
10. McDowell, L. M., Barkan, D., Wilson, G. E., and Schaefer, J. (1996) *Solid State Nucl. Magn. Reson. 7*, 203−210.
11. Gullion, T., and Schaefer, J. (1989) *J. Magn. Reson. 81*, 196−200.
12. Gullion, T., and Schaefer, J. (1989) *Adv. Magn. Reson. 13*, 58−83.
13. Li, Y., Poliks, B., Cegelski, L., Poliks, M., Gryczynski, Z., Piszcek, G., Jagtap, P. G., Studelska, D. R., Kingston, D. G. I., Schaefer, J., and Bane, S. (2000) *Biochemistry 39*, 281−291.
14. Balbach, J. J., Ishii, Y., Antzutkin, O. N., Leapman, R. D., Rizzo, N. W., Dyda, F., Reed, J., and Tycko, R. (2000) *Biochemistry 39*, 13748−13759.
15. Smith, S. O., Kawakami, T., Liu, W., Ziliox, M., and Aimoto, S. (2001) *J. Mol. Biol. 313*, 1139−1148.
16. Murphy, O. J., III, Kovacs, F. A., Sicard, E., and Thompson, L. K. (2001) *Biochemistry 40*, 1358−1366.
17. Merritt, M. E., Christensen, A. M., Kramer, K. J., Hopkins, T. L., and Schaefer, J. (1996) *J. Am. Chem. Soc. 118*, 11278−11282.
18. Tong, G., Pan, Y., Dong, H., Pryor, R., Wilson, G. E., and Schaefer, J. (1997) *Biochemistry 36*, 9859−9866.
19. Michal, C. A., and Jelinski, L. W. (1998) *J. Biomol. NMR 12*, 231−241.
20. Schaefer, J., and McKay, R. M. (1999) U.S. Patent 5,861,748.
21. Holl, S. M., Marshall, G. R., Beusen, D. D., Kociolek, K., Redlinski, A. S., Leplawy, M T., McKay, R. A., Vega, S., and Schaefer, J. (1992) *J. Am. Chem. Soc. 114*, 4830−4833.
22. Gullion, T., Baker, D. B., and Conradi, M. S. (1990) *J. Magn. Reson. 89*, 479−484.
23. Ream, J. E., Yuen, H. K., Frazier, R. B., and Sikorski, J. A. (1992) *Biochemistry 31*, 5528−5534.
24. Jencks, W. P. (1997) *Annu. Rev. Biochem. 66*, 1−18.
25. Blow, D. (2000) *Structure 8*, R77−R81.
26. Eyring, H., Lumry, R., and Spikes, J. D. (1954) in *Mechanisms of Enzyme Action* (McElroy, W., and Glass, B., Eds.) p 123, Johns Hopkins University Press, Baltimore, MD.
27. Bruice, T. C., and Benkovic, S. J. (2000) *Biochemistry 39*, 6267−6274.
28. Lumry, R. (1995) in *Protein−Solvent Interactions* (Gregory, R., Ed.) pp 12−28, Marcel Dekker, New York, NY.
29. Stone, M. J. (2001) *Acc. Chem. Res. 34*, 379−388.

BI049685W